Supplementary Material

Supplementary Figure S1.

Results of the ISOLA modelling of the mainshock (top panel) and plots with synthetic vs. observed waveforms (bottom panel) showing the quality of the fit.

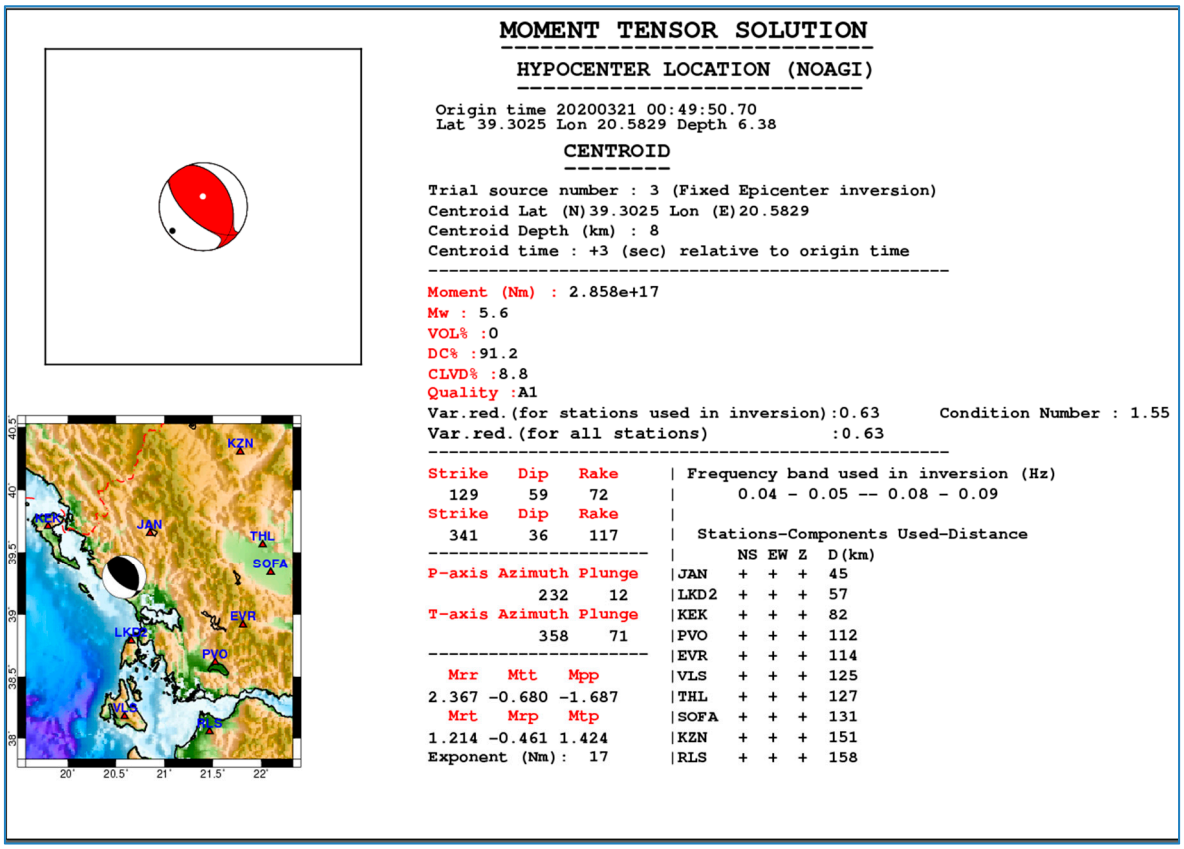

Supplementary Figure S2.

(Top) Map of the relocated 2020 Kanallaki earthquake sequence. The relocated catalogue was divided in six spatial groups (see colours and numerical labels) using Ward's linkage on the matrix of 2D inter-event epicentral distances, to provide visual aid for the cross-section description.

(Bottom) Cross-sections along the profiles a1-a2 (in a SW-NE direction) and b1-b2 (in a NW-SE direction) shown on the map. Stars represent the larger events, with $M_L \geq 3.5$. The topography is also presented at the top of the cross-sections (without vertical exaggeration).

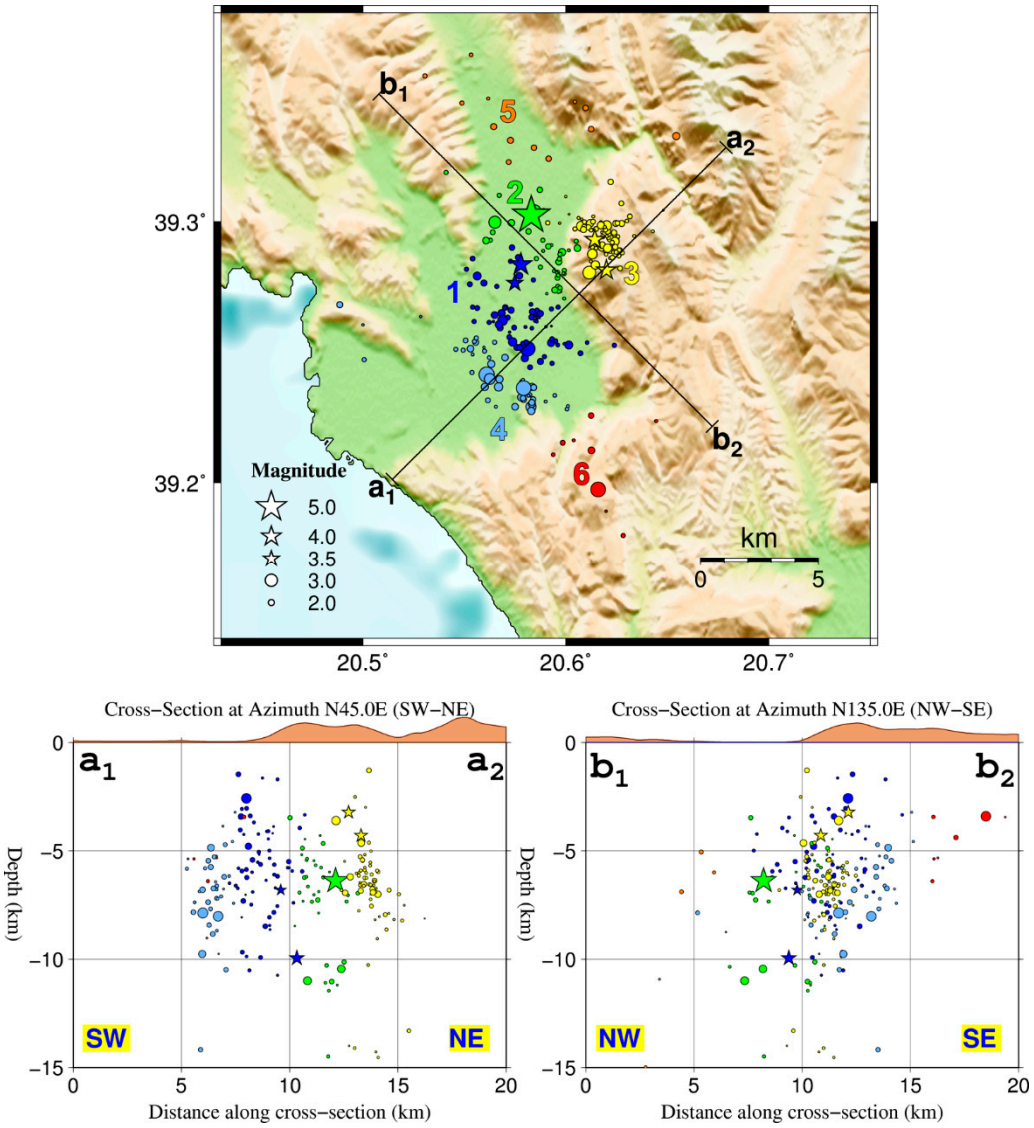

Supplementary Figure S3.

Map showing the Sentinel-1 frames with data used in this paper. Yellow star denotes the epicentre of the Kanallaki earthquake.

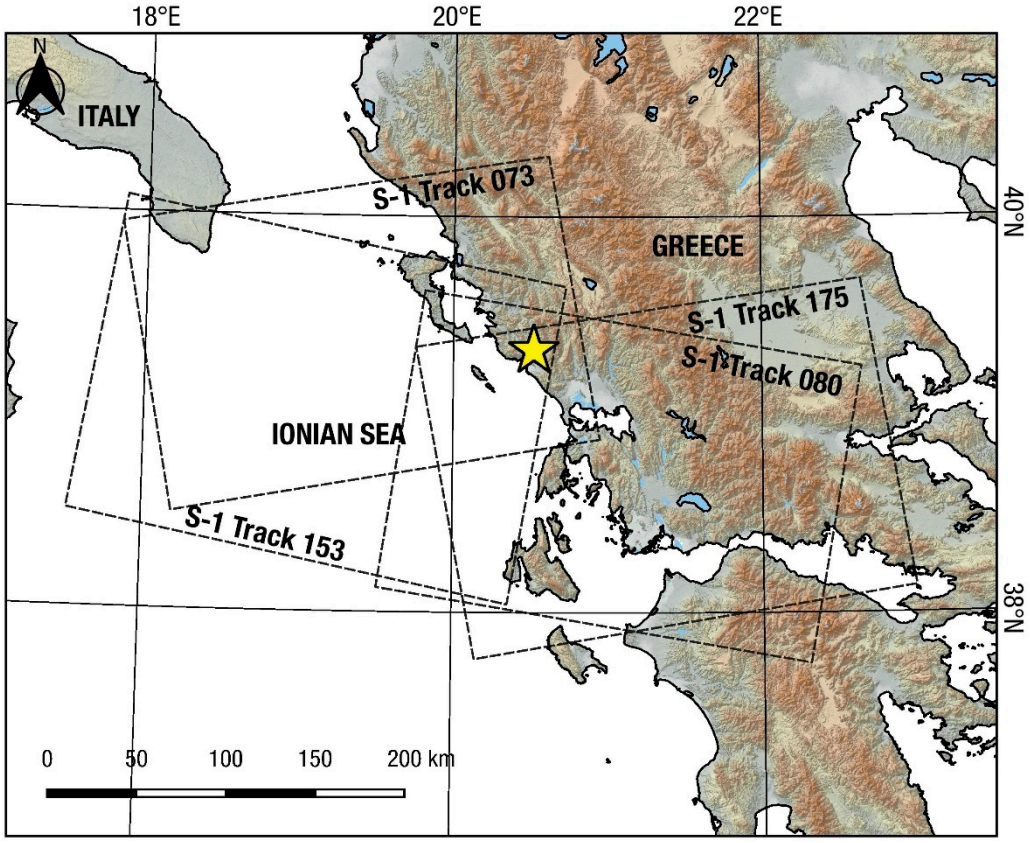

Supplementary Figure S4.

Coseismic interferograms for the Kanallaki earthquake that were not used in the inversion due to low quality and noise. Dates of image pairs are reported on the lower left part of the images.

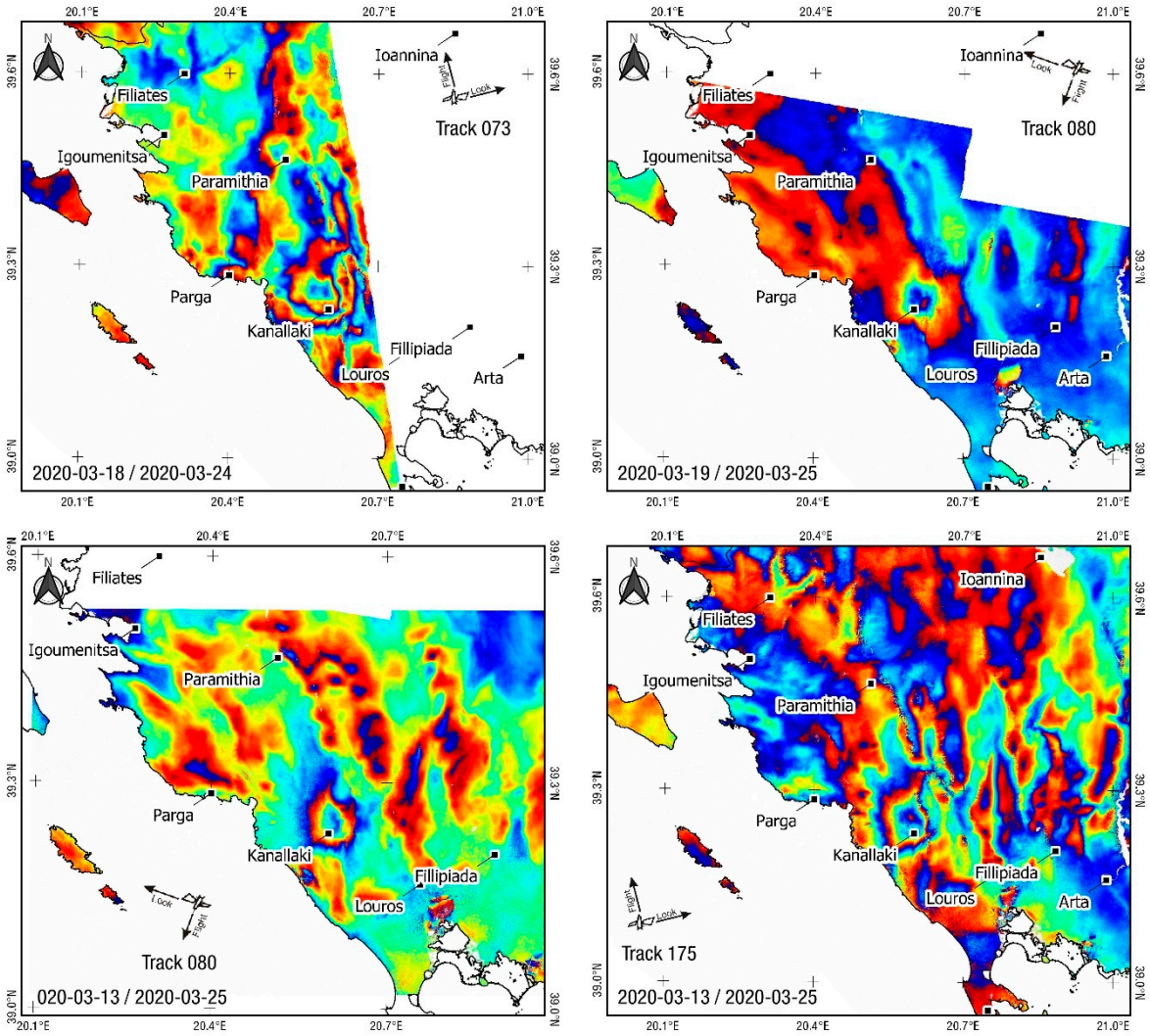

Supplementary Figure S5.

Graph of the Global Navigation Satellite System (GNSS) time series of station GARD detrended of its long-term velocity (top-panel: Up component, mid-panel: North component, and bottom-panel: East component). The post-seismic data is enough to estimate the amplitude of the co-seismic motion. This amplitude is –3.2 ± 0.2 mm in east, 0.2 ± 0.2 mm in north, and 0.3 ± 0.5 mm in Up. The modelled amplitude of displacement with our current fault model is –1.1 mm in east, 1.7 mm in north, and 0.3 mm in Up. Those numbers are very small.

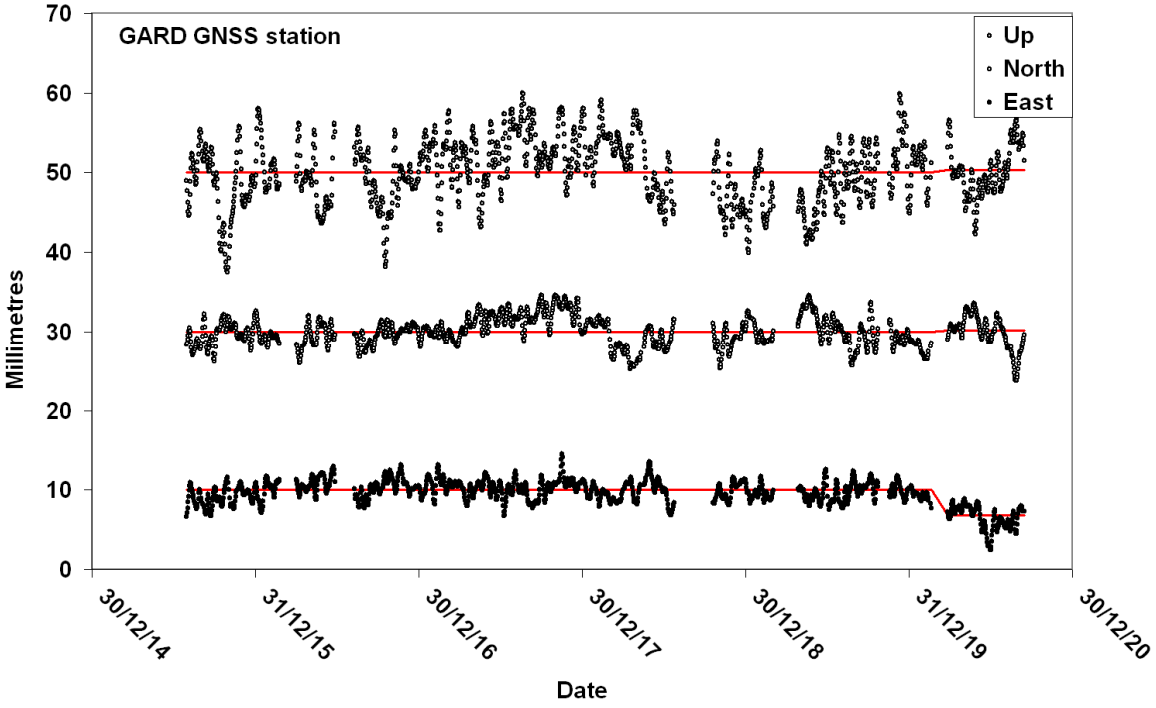

Supplementary Figure S6.

Aerial overview of the earthquake epicentre area. Picture made by A. Ganas on September 27, 2019 on the flight Athens to Brussels. View towards WSW. Kanallaki is on the southern (left) side of the picture. Note the Lippa mountain with V-shaped orthogonal valleys facing the village of Gardiki. Lippa forms an anticline structure immediately west of Gardiki and the Kokitos river valley. The azimuth of this geological structure is N335°E. The Acherontas is river is located to the left of the Kokitos river (see Figure 9A for a map view).

Supplementary Figure S7

Intensity distribution for the 1895 earthquake (SHEEC epicentre with red star). Site names and EMS intensity values are described in Table S3. (B) Intensities near the epicentre of the 1895 earthquake for the area outlined with a dotted line in A.

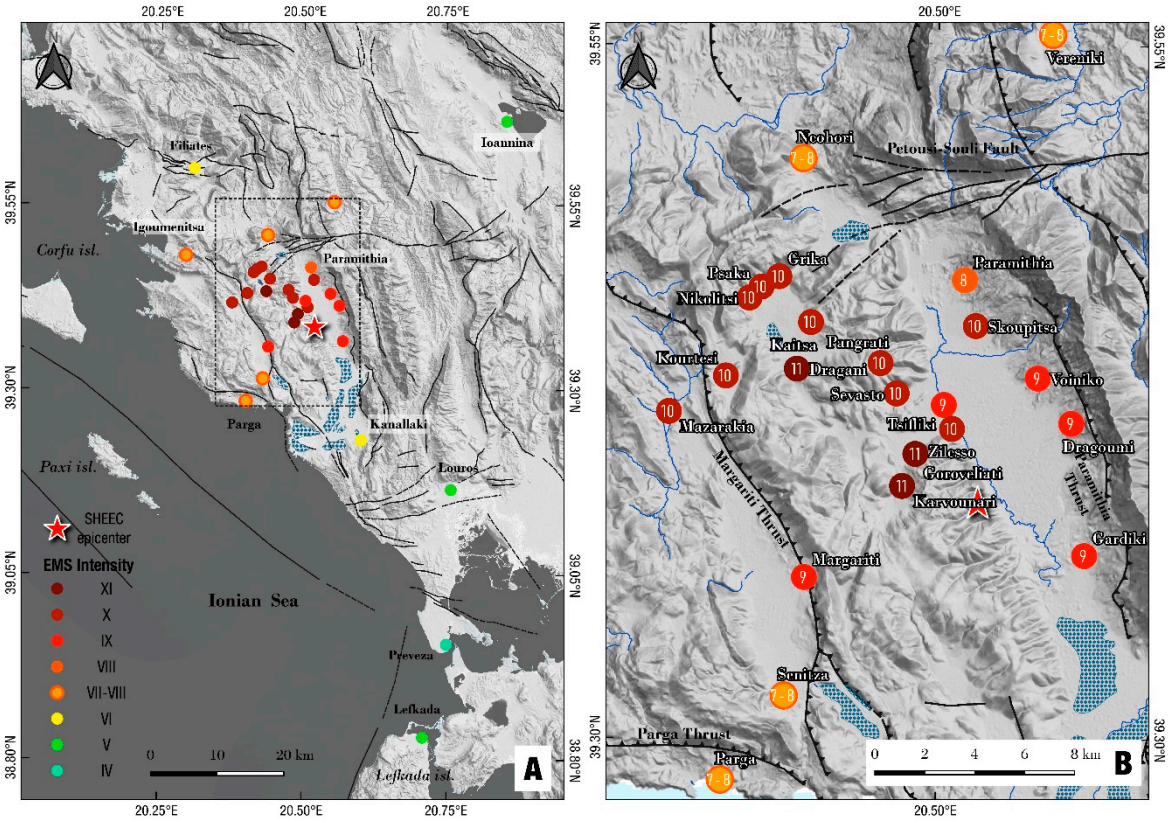

Supplementary Table S1.

Catalogue of strong events for the study area, 1915–2019 ($M_L \geq 5.2$; source Makropoulos et al. 2012; reference 26 in the main text).

YEAR	MONTH	DAY	HOUR	MIN	SEC	LAT	LON	DEP	Mw
1915	2	20	8	13	0	39.200	20.500	30	5.2
1920	10	21	18	57	51.7	39.430	20.360	10	5.6
1935	9	3	17	35	39.3	39.450	20.670	106	5.3
1938	3	11	14	51	6.1	39.230	20.520	55	5.2
1945	1	8	22	42	23.3	39.170	20.470	53	5.3
1968	3	28	16	37	47.3	39.490	20.380	18	5.2
1972	11	24	3	48	34.2	39.390	20.430	9	5.3
1979	11	6	5	26	16	39.560	20.320	26	5.6
1979	11	11	1	18	6.3	39.520	20.300	27	5.3
1981	7	3	21	42	57.7	39.540	20.670	25	5.2
1990*	6	16	2	16	21.1	39.160	20.540	7	5.5
1993	6	13	23	26	40.3	39.340	20.530	20	5.6
2007	6	29	18	9	12.65	39.297	20.249	17.6	5.4

* from Louvari et al. (2001), reference 8 in the main text.

Supplementary Table S2.

Observed values (fringe picking) and modelled values (in mm). The first 86 values are for the ascending interferogram and the following 86 for the descending.

N°	UTM34-East (km)	UTM34-North (km)	Observed displacement along the line of sight	Model
1	464.88	4343.1	34	29.64
2	464.98	4342	34	25.97
3	464.98	4342.8	34	28.83
4	465.08	4342.4	34	27.52
5	465.08	4342.5	34	27.87
6	465.08	4342.6	34	28.21
7	462.98	4342.9	27	24.64
8	463.38	4341.4	27	20.54
9	463.38	4341.5	27	20.95
10	463.48	4345.4	27	28.83
11	463.58	4341.5	27	21.5
12	463.68	4343.7	27	29
13	463.78	4345.9	27	28.51
14	463.78	4346.7	27	26.06
15	463.98	4346.9	27	25.5
16	464.18	4344.1	27	30.71
17	464.18	4347.2	27	24.37
18	464.58	4340.7	27	19.95
19	465.08	4343.6	27	30.72
20	465.88	4347.1	27	22.63
21	465.98	4343.8	27	29.7
22	466.08	4343.9	27	29.51
23	466.08	4344	27	29.55
24	466.08	4346.4	27	24.93
25	466.68	4347.6	27	18.03
26	466.88	4342.9	27	25.67
27	461.08	4347.3	20	16.9
28	461.28	4346.1	20	19.61
29	461.38	4347.3	20	17.92
30	461.88	4342.1	20	17.71
31	462.28	4340.2	20	12.84
32	462.28	4347.6	20	19.84
33	462.28	4347.8	20	19.18
34	462.38	4340.8	20	15.18
35	462.68	4341.4	20	18.34
36	462.68	4341.5	20	18.71

37	462.88	4341.2	20	18.23
38	462.88	4341.3	20	18.62
39	462.88	4344	20	26.7
40	463.38	4348.3	20	19.13
41	463.58	4339.6	20	13.74
42	463.58	4339.7	20	14.12
43	464.28	4348.5	20	18.47
44	467.18	4341.8	20	21.91
45	467.28	4342.9	20	24.14
46	467.38	4341.9	20	21.53
47	464.18	4349.8	13	12.91
48	466.08	4349.7	13	10.99
49	464.68	4349.5	13	13.78
50	462.78	4349.3	13	14.56
51	466.08	4348.9	13	14.14
52	465.98	4348.6	13	15.65
53	460.58	4347.4	13	14.99
54	467.28	4347	13	18.21
55	459.98	4345.7	13	14.3
56	459.98	4345.6	13	14.31
57	460.48	4344.5	13	16.1
58	460.08	4343.9	13	13.72
59	468.18	4343.7	13	20.62
60	468.58	4342.8	13	18.2
61	468.08	4342	13	19.14
62	465.58	4340.1	13	17.82
63	462.68	4339	13	9.98
64	464.08	4338.8	13	11.62
65	464.08	4338.7	13	11.28
66	465.18	4338.6	13	11.84
67	456.38	4347.5	6	4.2
68	456.78	4347.6	6	4.84
69	457.18	4353	6	2.57
70	458.28	4353.1	6	3.07
71	458.68	4352.7	6	3.62
72	459.18	4341.8	6	7.35
73	459.78	4348.6	6	10.63
74	460.08	4352	6	5.33
75	460.78	4352.3	6	5.28
76	461.28	4339.1	6	7.36
77	461.88	4338.8	6	7.87
78	464.18	4336.1	6	4.85
79	465.68	4350.7	6	8.25

80	466.68	4349.5	6	10.51
81	467.68	4340.4	6	16.06
82	468.48	4339.6	6	11.85
83	469.08	4339.3	6	9.83
84	469.48	4340.6	6	11.35
85	469.68	4339.1	6	8.19
86	455.68	4346.6	6	3.13
87	467.78	4345.63	31.5	26.94
88	465.68	4345.53	31.5	28.82
89	465.78	4345.43	31.5	29.24
90	465.08	4345.23	31.5	28.07
91	465.28	4345.23	31.5	28.65
92	465.58	4345.23	31.5	29.36
93	465.58	4345.03	31.5	29.73
94	465.98	4344.93	31.5	30.57
95	465.98	4344.83	31.5	30.72
96	466.48	4344.73	31.5	31.21
97	466.98	4344.73	31.5	30.95
98	467.48	4344.73	31.5	30.12
99	466.88	4344.43	31.5	31.44
100	466.78	4344.33	31.5	31.59
101	465.88	4344.23	31.5	31.04
102	465.78	4343.13	31.5	29.65
103	465.78	4343.03	31.5	29.42
104	466.68	4342.13	31.5	28.13
105	466.28	4346.73	24.5	24.72
106	467.68	4346.73	24.5	22.69
107	466.28	4346.63	24.5	25.17
108	467.68	4346.63	24.5	23.15
109	466.08	4346.53	24.5	25.6
110	467.38	4346.43	24.5	24.76
111	466.28	4346.33	24.5	26.48
112	466.58	4346.23	24.5	26.78
113	464.88	4343.43	24.5	27.31
114	464.08	4343.33	24.5	23.44
115	464.98	4343.33	24.5	27.52
116	464.58	4342.93	24.5	24.94
117	467.88	4342.33	24.5	28.07
118	467.88	4342.23	24.5	27.81
119	464.38	4341.83	24.5	20.73
120	464.48	4341.83	24.5	21.15
121	464.68	4341.63	24.5	21.23
122	464.78	4341.63	24.5	21.61

123	466.48	4341.23	24.5	24.39
124	466.08	4349.43	17.5	11.89
125	466.58	4349.13	17.5	12.89
126	466.28	4348.93	17.5	14.01
127	466.38	4348.93	17.5	13.95
128	466.38	4348.83	17.5	14.41
129	466.18	4348.73	17.5	14.99
130	465.68	4348.23	17.5	17.4
131	465.78	4348.23	17.5	17.42
132	467.48	4348.03	17.5	16.84
133	467.78	4348.03	17.5	16.2
134	467.48	4347.93	17.5	17.33
135	467.88	4347.93	17.5	16.45
136	468.48	4347.33	17.5	17.58
137	463.88	4346.33	17.5	21.05
138	463.28	4343.23	17.5	19.1
139	463.58	4341.63	17.5	16.64
140	467.58	4341.63	17.5	26.27
141	463.98	4340.73	17.5	15.37
142	465.88	4340.73	17.5	21.18
143	466.18	4339.93	17.5	18.28
144	466.48	4339.93	17.5	18.72
145	462.38	4343.43	10.5	14.75
146	462.48	4343.63	10.5	15.49
147	462.58	4343.53	10.5	15.88
148	462.98	4346.43	10.5	16.91
149	462.98	4344.23	10.5	18.65
150	463.08	4346.03	10.5	18.12
151	463.68	4347.93	10.5	15.26
152	463.78	4347.13	10.5	18.29
153	463.78	4339.93	10.5	12.17
154	463.88	4347.03	10.5	18.96
155	463.88	4339.93	10.5	12.47
156	463.98	4339.93	10.5	12.77
157	464.08	4347.83	10.5	16.71
158	464.18	4339.83	10.5	13.05
159	464.38	4339.83	10.5	13.63
160	464.98	4349.33	10.5	12.11
161	464.98	4349.23	10.5	12.52
162	465.28	4349.43	10.5	11.88
163	465.58	4350.43	10.5	8.21
164	465.98	4338.83	10.5	13.6
165	466.18	4338.83	10.5	13.89

166	466.48	4350.53	10.5	7.52
167	466.58	4350.53	10.5	7.44
168	466.78	4350.43	10.5	7.61
169	467.08	4350.33	10.5	7.65
170	467.18	4350.53	10.5	6.89
171	467.58	4349.93	10.5	8.42
172	467.78	4349.63	10.5	9.23

Supplementary Table S3.

Intensity observations for the 1895 earthquake near Dragani (Fig. 4). QIa refers to the quality of the respective intensity observation, i.e. A = reliable, B = fair, and C = uncertain.

Site Name	Latitude	Longitude	Intensity EMS	QIa
Dragani	39.4333	20.4345	11	A
Goroveliati	39.4028	20.4899	11	B
Karvounari	39.3912	20.4837	11	A
Grika	39.4666	20.4261	10	B
Kaitsa	39.4501	20.4410	10	B
Kourtesi	39.4307	20.4015	10	B
Mazarakia	39.4177	20.3751	10	B
Nikolitsi	39.4588	20.4123	10	B
Pangrati	39.4355	20.4734	10	B
Psaka	39.4628	20.4178	10	B
Sevasto	39.4246	20.4810	10	B
Skoupitsa	39.4490	20.5177	10	B
Zilesso	39.4119	20.5068	10	B
Dragoumi	39.4139	20.5623	9	B
Gardiki	39.3662	20.5685	9	B
Margariti	39.3582	20.4384	9	C
Tsifliki	39.4205	20.503	9	B
Voiniko	39.4302	20.5466	9	B
Paramithia	39.4655	20.5124	8	C
Grekohori	39.4816	20.2942	7–8	B
Neohori	39.5092	20.4370	7–8	B
Parga	39.2850	20.4000	7–8	C
Senitza	39.3154	20.4293	7–8	C
Vereniki	39.5541	20.5530	7–8	C
Filiates	39.5991	20.3081	6	C
Kanallaki	39.2323	20.6006	6	C
Ioannina	39.6635	20.8542	5	C
Lefkada	38.8304	20.7086	5	C
Louros	39.1654	20.7573	5	C
Preveza	38.9562	20.7497	4	C

Supplementary Table S4.

Variability of the solution as a function of the focal mechanism parameters. We report the best fitting models obtained when using strictly the three angles reported in Table 3 by various agencies. This shows that there is no major difference between the various models. The definition of the zero value of the interferogram has more impact on the model than the selection of a particular focal mechanism solution among those available.

Source	**Centroid (UTM34)**				
	Long.	**Lat.**	**Depth**	**Fault length**	**Geodetic moment tensor**
	km	km	km	km	* 10^{17} N m
GCMT	465.17	4345.32	7.57	4.58	2.40
GFZ	465.84	4344.03	7.25	4.44	2.33
IPGP	465.65	4344.60	7.19	4.42	2.32
USGS	465.20	4343.23	7.26	4.14	2.17
NOA	466.09	4344.74	7.39	4.78	2.51
AUTH	465.39	4344.74	7.21	4.30	2.26
INGV	465.15	4344.61	7.32	4.26	2.24
Average	**465.50**	**4344.47**	**7.31**	**4.42**	**2.32**
Standard deviation	**0.37**	**0.66**	**0.13**	**0.21**	**0.11**

Supplementary Table S5.

Co-seismic landslides for the Mw = 5.6 March 21, 2020 earthquake. The table includes 17 locations where co-seismic landslides were identified using cloud-free pre- and post-seismic Copernicus Sentinel-2 optical imagery (10-m resolution). Locations are shown in Figure 10a.

ID	East (UTM34N) (m)	North (UTM34N) (m)	Longitude (°)	Latitude (°)
1	465,120	4,340,835	20.5959	39.2160
2	465,531	4,340,784	20.6007	39.2156
3	465,465	4,340,661	20.5999	39.2145
4	466,619	4,340,472	20.6133	39.2128
5	466,202	4,339,220	20.6085	39.2015
6	466,189	4,338,929	20.6084	39.1989
7	466,206	4,339,018	20.6086	39.1997
8	465,471	4,349,038	20.5996	39.2900
9	471,122	4,349,479	20.6651	39.2942
10	471,250	4,349,340	20.6666	39.2929
11	471,133	4,348,849	20.6652	39.2885
12	467,926	4,343,121	20.6283	39.2368
13	467,908	4,342,958	20.6281	39.2353
14	469,467	4,343,838	20.6461	39.2433
15	467,841	4,343,526	20.6273	39.2404
16	467,714	4,342,908	20.6259	39.2348
17	467,530	4,343,329	20.6237	39.2386